

# The $\Lambda(1405)$ in resummed chiral effective field theory

Xiu-Lei Ren <sup>1</sup>, E. Epelbaum <sup>2</sup>, J. Gegelia <sup>2,3</sup> and U.-G. Meißner <sup>4,5,3</sup>

<sup>1</sup>*Institut für Kernphysik & Cluster of Excellence PRISMA<sup>+</sup>,*

*Johannes Gutenberg-Universität Mainz, D-55128 Mainz, Germany*

<sup>2</sup>*Institut für Theoretische Physik II, Ruhr-Universität Bochum, D-44780 Bochum, Germany*

<sup>3</sup>*Tbilisi State University, 0186 Tbilisi, Georgia*

<sup>4</sup>*Helmholtz Institut für Strahlen- und Kernphysik and Bethe Center for Theoretical Physics,*

*Universität Bonn, D-53115 Bonn, Germany*

<sup>5</sup>*Institute for Advanced Simulation, Institut für Kernphysik and Jülich Center for Hadron Physics,*

*Forschungszentrum Jülich, D-52425 Jülich, Germany*

## Abstract

We study the unitarized meson-baryon scattering amplitude at leading order in the strangeness  $S = -1$  sector using time-ordered perturbation theory for a manifestly Lorentz-invariant formulation of chiral effective field theory. By solving the coupled-channel integral equations with the full off-shell dependence of the effective potential and applying subtractive renormalization, we analyze the renormalized scattering amplitudes and obtain the two-pole structure of the  $\Lambda(1405)$  resonance. We also point out the necessity of including higher-order terms.

## I. INTRODUCTION

With the breakthrough in the observation of gravitational waves by the Advanced LIGO and Virgo Collaborations [1], the study of neutron stars enters a new era of multi-message observations. As the density increases, the strange degrees of freedom are expected to become active in the interior of dense objects like e.g. neutron stars. In addition to the appearance of hyperons, antikaon condensation can soften the equation of state and modify the bulk properties of neutron stars [2, 3]. Besides, bound systems of antikaonic and multi-antikaonic nuclei have been studied e.g. in Ref. [4]. Those phenomena attract attention to studying the dynamics of the strong  $\bar{K}N$  interaction. Such investigations are also essential to deepen our understanding of the SU(3) dynamics in nonperturbative QCD.

The interaction of  $\bar{K}N$  is rather strong as manifested in the existence of the  $\Lambda(1405)$  resonance [5] close to the  $\bar{K}N$  threshold. The  $\Lambda(1405)$  resonance was first predicted by Dalitz and Tuan [6], and it has been confirmed soon after by hydrogen bubble chamber experiments in the analysis of the  $\pi\Sigma$  mass spectrum [7, 8]. Since its discovery many studies have been carried out to uncover the nature of the  $\Lambda(1405)$  resonance. From the experimental side, a large amount of  $K^-p$  data are available such as the total cross sections for the processes  $K^-p \rightarrow \{K^-p, \bar{K}^0n, \pi^0\Sigma^0, \pi^+\Sigma^-, \pi^-\Sigma^+\}$  [9–12], the ratios of  $K^-p$  capture rates [13, 14], and the measurement of the characteristics of kaonic hydrogen constraining the  $K^-p$   $S$ -wave scattering length in the SIDDHARTA experiment [15]. The  $\Lambda(1405)$  has been investigated within a variety of theoretical approaches, e.g., the relativistic quark model [16], QCD sum rules [17], phenomenological potential models [18–22], the Skyrme model [23], the Hamiltonian effective field theory [24], and the chiral unitary approach [25–42]. Detailed discussions can be found in recent review articles, see, e.g., Refs. [43–46], and in the review section of PDG [5]. Besides, the  $\Lambda(1405)$  resonance has also been studied in lattice QCD simulations [47–49].

Among the above mentioned theoretical methods, the chiral unitary approach that relies on chiral perturbation theory [50, 51] retains a special place as it incorporates important constraints from the chiral symmetry on the dynamical generation of  $\Lambda(1405)$ . The most-interesting phenomenon of the two-pole structure of  $\Lambda(1405)$ , i.e. that two poles are found on the same Riemann sheet, was first reported in Ref. [27]. The origin of this two-pole structure is attributed to the two attractive channels ( $\pi\Sigma$  and  $\bar{K}N$ ) in the SU(3) basis. Details of the two-pole structure can be found in the dedicated review article [52]. Various studies have revealed that the higher pole (i.e. the one with

the larger real part) is slightly below the threshold of  $\bar{K}N$  with the narrow width of the order of 10 MeV. However, for the lower pole of  $\Lambda(1405)$ , there is about 50 MeV uncertainty in the real and imaginary parts obtained in different works [35–39], because the current experimental data are not very sensitive to the lower pole. This raised a debate on the one-pole versus two-pole structure of  $\Lambda(1405)$  state, see, e.g., Refs. [53–57]. Note that the mentioned studies finding only a single pole have some deficiencies as detailed e.g. in Ref. [52]. Notice further that in chiral unitary models, the scattering amplitudes depend on the momentum cutoff parameter ( $\Lambda$ ) [26] or subtraction constant(s) [27, 33, 43] introduced to deal with the ultraviolet divergences in the unitarization procedure. This results in some model dependence of the pole position(s) of the  $\Lambda(1405)$ .

Recently we have proposed a renormalizable approach to study meson-baryon scattering by utilizing time-ordered perturbation theory for a manifestly Lorentz-invariant formulation of chiral perturbation theory [58]. Effective potentials are defined as the sums of all possible two-particle irreducible time-ordered diagrams, and the integral equations for the meson-baryon scattering amplitudes are derived in time-ordered perturbation theory. Renormalized amplitudes are obtained by applying the subtractive renormalization to the solutions of the integral equations at leading order (LO), while higher-order corrections are included perturbatively in a similar fashion to Refs. [59–61]. As shown in Ref. [58], our approach can be successfully applied to the pion-nucleon system. In the current work, we apply this framework to study meson-baryon systems with strangeness  $S = -1$  at LO and investigate the nature of the S-wave  $\Lambda(1405)$  resonance. This study should be considered as a first step. In the future, we plan to extend it to include higher-order corrections and further experimental data in order to sharpen our conclusions.

The manuscript is organized as follows. In Sect. II we lay out the formalism to study meson-baryon scattering in SU(3) unitarized chiral effective field theory based on a renormalizable approach. Our results are presented and discussed in Sect. III. We end with a summary and outlook in Sect. IV.

## II. THEORETICAL FRAMEWORK

In this section we briefly outline the theoretical framework of our work, which is the three-flavor extension of the SU(2) formalism developed in Ref. [58].

### A. Meson-baryon scattering amplitude

The on-shell amplitude of the elastic meson-baryon scattering process  $M_1(q_1) + B_1(p_1) \rightarrow M_2(q_2) + B_2(p_2)$  can be parameterized as

$$\begin{aligned} T_{MB} &= \bar{u}_{B_2}(p_2, s_2) \left[ A + \frac{1}{2}(\not{q}_1 + \not{q}_2)B \right] u_{B_1}(p_1, s_1) \\ &= \bar{u}_{B_2}(p_2, s_2) \left[ D + \frac{i}{m_{B_1} + m_{B_2}} \sigma^{\mu\nu} q_{2,\mu} q_{1,\nu} B \right] u_{B_1}(p_1, s_1), \end{aligned} \quad (1)$$

with  $\sigma^{\mu\nu} = \frac{i}{2}[\gamma^\mu, \gamma^\nu]$ , and  $D = A + B(s - u)/(2(m_{B_1} + m_{B_2}))$ . The conventional Mandelstam variables are defined as  $s = (p_1 + q_1)^2$ ,  $t = (p_1 - p_2)^2$ , and  $u = (p_1 - q_2)^2$  with  $s + t + u = M_{M_1}^2 + m_{B_1}^2 + M_{M_2}^2 + m_{B_2}^2$ . The Dirac spinor  $u(p, s)$  of a baryon is normalized according to

$$u_B(p, s) = \sqrt{\frac{\omega_B(p) + m}{2m}} \begin{pmatrix} 1 \\ \frac{\boldsymbol{\sigma} \cdot \mathbf{p}}{\omega_B(p) + m} \end{pmatrix} \chi_s, \quad (2)$$

where  $\chi_s$  is a two-component spinor with spin  $s$ , and  $\omega_B(p) = \sqrt{\mathbf{p}^2 + m^2}$  is the energy. Following Ref. [58], we decompose the Dirac spinor as

$$u_B(p) = u_0 + [u(p) - u_0] \equiv \begin{pmatrix} 1 \\ 0 \end{pmatrix} \chi_s + u_{\text{ho}}, \quad (3)$$

and consider  $u_{\text{ho}}$  as a higher-order contribution. Using the leading approximation for the Dirac spinor we obtain the reduced amplitude which reads

$$\begin{aligned} T_{MB} &= D - \frac{\mathbf{q}_1 \cdot \mathbf{q}_2}{m_{B_1} + m_{B_2}} B + \frac{(\boldsymbol{\sigma} \cdot \mathbf{q}_2)(\boldsymbol{\sigma} \cdot \mathbf{q}_1)}{m_{B_1} + m_{B_2}} B \\ &\equiv T_{MB}^c + i \boldsymbol{\sigma} \cdot (\mathbf{q}_2 \times \mathbf{q}_1) T_{MB}^{so}, \end{aligned} \quad (4)$$

where we have introduced the non-spin-flip amplitude  $T_{MB}^c$  and the spin-flip amplitude  $T_{MB}^{so}$ .

### B. The leading-order effective Lagrangian and the meson-baryon interaction potential

Below we present the LO potential of the meson-baryon interaction in the strangeness  $S = -1$  sector and the corresponding scattering equation obtained using time-ordered perturbation theory within a manifestly Lorentz-invariant chiral effective Lagrangian. The details of the formalism can be found in Ref. [58]. To keep the paper self-contained we provide below the basic ingredients of the three-flavor extension used here.

One essential feature of our framework is that it incorporates the fields corresponding to lowest-lying vector mesons as dynamical degrees of freedom of the effective Lagrangian. In this formulation, the Weinberg-Tomozawa term in the effective meson-baryon Lagrangian is saturated by the vector-meson exchange, which has a better ultraviolet behavior. The LO chiral Lagrangian used in our calculations has the form

$$\begin{aligned} \mathcal{L}_{\text{LO}} = & \frac{F_0^2}{4} \langle u_\mu u^\mu + \chi_+ \rangle + \langle \bar{B} (i\gamma_\mu \partial^\mu - m) B \rangle + \frac{D/F}{2} \langle \bar{B} \gamma_\mu \gamma_5 [u^\mu, B]_\pm \rangle \\ & - \frac{1}{4} \left\langle V_{\mu\nu} V^{\mu\nu} - 2M_V^2 \left( V_\mu - \frac{i}{g} \Gamma_\mu \right) \left( V^\mu - \frac{i}{g} \Gamma^\mu \right) \right\rangle + g \langle \bar{B} \gamma_\mu [V^\mu, B] \rangle, \end{aligned} \quad (5)$$

where  $\langle \dots \rangle$  denotes the trace in the flavor space, and

$$\begin{aligned} u_\mu &= i(u^\dagger \partial_\mu u - u \partial_\mu u^\dagger), \quad u = \exp \left( i P / (\sqrt{2} F_0) \right), \\ \chi_+ &= u^\dagger \chi u^\dagger + u \chi^\dagger u, \quad \text{with } \chi = 2B_0 \mathcal{M}, \\ \Gamma_\mu &= \frac{1}{2} (u^\dagger \partial_\mu u + u \partial_\mu u^\dagger), \\ V_{\mu\nu} &= \partial_\mu V_\nu - \partial_\nu V_\mu - ig[V_\mu, V_\nu], \end{aligned} \quad (6)$$

with the pion decay constant  $F_0$  in the three-flavor chiral limit, and  $D$  and  $F$  - the axial-vector couplings. We use the coupling constant of the vector-field self-interaction  $g$  determined via the KSFR relation,  $M_V^2 = 2g^2 F_0^2$ .  $\mathcal{M}$  denotes the quark-mass matrix and  $B_0$  is related to the scalar quark condensate,  $m$  and  $M_V$  stand for the octet baryon and the vector meson masses in the chiral limit, respectively. The SU(3) matrices collecting the pseudoscalar mesons, the octet baryons and the vector mesons are given, respectively, by

$$\begin{aligned} P &= \begin{pmatrix} \frac{1}{\sqrt{2}}\pi^0 + \frac{1}{\sqrt{6}}\eta & \pi^+ & K^+ \\ \pi^- & -\frac{1}{\sqrt{2}}\pi^0 + \frac{1}{\sqrt{6}}\eta & K^0 \\ K^- & \bar{K}^0 & -\frac{2}{\sqrt{6}}\eta \end{pmatrix}, \\ B &= \begin{pmatrix} \frac{1}{\sqrt{2}}\Sigma^0 + \frac{1}{\sqrt{6}}\Lambda & \Sigma^+ & p \\ \Sigma^- & -\frac{1}{\sqrt{2}}\Sigma^0 + \frac{1}{\sqrt{6}}\Lambda & n \\ \Xi^- & \Xi^0 & -\frac{2}{\sqrt{6}}\Lambda \end{pmatrix}, \\ V_\mu &= \begin{pmatrix} \frac{\rho^0}{\sqrt{2}} + \frac{\omega}{\sqrt{2}} & \rho^+ & K^{*+} \\ \rho^- & -\frac{\rho^0}{\sqrt{2}} + \frac{\omega}{\sqrt{2}} & K^{*0} \\ K^{*-} & \bar{K}^{*0} & \phi \end{pmatrix}_\mu. \end{aligned} \quad (7)$$

At leading order, the meson-baryon scattering amplitude for the process  $M_i(q_1) + B_i(p_1) \rightarrow M_j(q_2) + B_j(p_2)$  is given by the time-ordered diagrams shown in Fig. 1. Besides the Born and

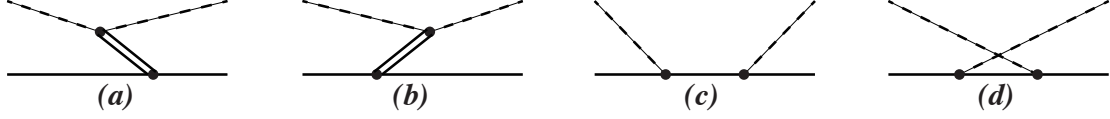


Figure 1: Time-ordered diagrams contributing to the LO meson-baryon potential. The dashed, solid and double-solid lines correspond to pseudoscalar mesons, octet baryons and vector mesons, respectively.

crossed-Born diagrams, there are also the vector meson exchange contributions that replace the Weinberg-Tomozawa contact term. Notice that the contributions stemming from the second term in the vector meson propagator  $\propto g^{\mu\nu} - q^\mu q^\nu / M_V^2$  are suppressed compared to the ones of the first term for considered low-energy processes and need to be taken into account together with other higher-order corrections. We further emphasize that possible power-counting-breaking contributions stemming from the decays  $V \rightarrow PP$  [62] in loop diagrams can be absorbed in vertex corrections [63].

In this LO calculation we employ the scattering amplitudes in the isospin limit using the averaged masses for the mesons and baryons. The LO potential in the isospin formalism is given by

$$\begin{aligned}
V_{M_j B_j, M_i B_i}^{(a+b)} &= -\frac{1}{32F_0^2} \sum_V C_{M_j B_j, M_i B_i}^V \frac{M_V^2}{\omega_V(q_1 - q_2)} (\omega_{M_i}(q_1) + \omega_{M_j}(q_2)) \\
&\quad \times \left( \frac{1}{E - \omega_{B_i}(p_1) - \omega_V(q_1 - q_2) - \omega_{M_j}(q_2)} \right. \\
&\quad \left. + \frac{1}{E - \omega_{B_j}(p_2) - \omega_V(q_1 - q_2) - \omega_{M_i}(q_1)} \right), \\
V_{M_j B_j, M_i B_i}^{(c)} &= \frac{1}{4F_0^2} \sum_B C_{M_j B_j, M_i B_i}^B \frac{m_B}{\omega_B(P)} \frac{(\boldsymbol{\sigma} \cdot \mathbf{q}_2)(\boldsymbol{\sigma} \cdot \mathbf{q}_1)}{E - \omega_B(P)}, \\
V_{M_j B_j, M_i B_i}^{(d)} &= \frac{1}{4F_0^2} \sum_B \tilde{C}_{M_j B_j, M_i B_i}^B \frac{m_B}{\omega_B(K)} \frac{(\boldsymbol{\sigma} \cdot \mathbf{q}_1)(\boldsymbol{\sigma} \cdot \mathbf{q}_2)}{E - \omega_{M_i}(q_1) - \omega_{M_j}(q_2) - \omega_B(K)}, \quad (8)
\end{aligned}$$

Table I: Coefficients  $C_{M_j B_j, M_i B_i}^V$  of the vector meson exchange contributions in the strangeness  $S = -1$  sector with isospin  $I = 0$ .

$C^V$	$\pi\Sigma$	$\bar{K}N$	$\eta\Lambda$	$K\Xi$
$\pi\Sigma$	$C^\rho = -16$	$C^{K^*} = 2\sqrt{6}$	0	$C^{K^*} = -2\sqrt{6}$
$\bar{K}N$		$C^{\{\rho, \omega, \phi\}} = \{-6, -2, -4\}$	$C^{K^*} = -6\sqrt{2}$	0
$\eta\Lambda$			0	$C^{K^*} = 6\sqrt{2}$
$K\Xi$				$C^{\{\rho, \omega, \phi\}} = \{-6, -2, -4\}$

Table II: Coefficients  $C_{M_j B_j, M_i B_i}^B$  of the Born terms in the strangeness  $S = -1$  sector with isospin  $I = 0$ .

$C^B$	$\pi\Sigma$	$\bar{K}N$	$\eta\Lambda$	$K\Xi$
$\pi\Sigma$	$C^\Lambda = 4D^2$	$C^\Lambda = \sqrt{\frac{8}{3}}D(D+3F)$	$C^\Lambda = \frac{4}{\sqrt{3}}D^2$	$C^\Lambda = -\sqrt{\frac{8}{3}}D(D-3F)$
$\bar{K}N$		$C^\Lambda = \frac{2}{3}(D+3F)^2$	$C^\Lambda = \frac{2\sqrt{2}}{3}D(D+3F)$	$C^\Lambda = -\frac{2}{3}(D^2-9F^2)$
$\eta\Lambda$			$C^\Lambda = \frac{4}{3}D^2$	$C^\Lambda = -\frac{2\sqrt{2}}{3}D(D-3F)$
$K\Xi$				$C^\Lambda = \frac{2}{3}(D-3F)^2$

Table III: Coefficients  $\tilde{C}_{M_j B_j, M_i B_i}^B$  of the crossed-Born terms in the strangeness  $S = -1$  sector with isospin  $I = 0$ .

$\tilde{C}^B$	$\pi\Sigma$	$\bar{K}N$	$\eta\Lambda$	$K\Xi$
$\pi\Sigma$	$\tilde{C}^{\{\Lambda, \Sigma\}} = \{\frac{4D^2}{3}, -8F^2\}$	$\tilde{C}^N = \sqrt{6}(F^2 - D^2)$	$\tilde{C}^\Sigma = -\frac{4}{\sqrt{3}}D^2$	$\tilde{C}^\Xi = \sqrt{6}(D^2 - F^2)$
$\bar{K}N$		0	$\tilde{C}^N = \frac{\sqrt{2}(D^2-9F^2)}{3}$	$\tilde{C}^{\{\Lambda, \Sigma\}} = \{\frac{9F^2-D^2}{3}, 3(F^2 - D^2)\}$
$\eta\Lambda$			$\tilde{C}^\Lambda = \frac{4}{3}D^2$	$\tilde{C}^\Xi = \frac{\sqrt{2}}{3}(9F^2 - D^2)$
$K\Xi$				0

where the expressions are summed over all vector mesons  $V$  in the vector-meson-exchange contributions, and over the internal baryons  $B$  in the Born and crossed-Born terms. Further,  $E = \sqrt{s}$  is the total energy of the meson-baryon system, and  $P = q_1 + p_1 = q_2 + p_2$ ,  $K = p_1 - q_2 = p_2 - q_1$ . The on-shell energy of a particle is given by  $\omega_X(p) \equiv \sqrt{m_X^2 + \mathbf{p}^2}$ .

In the  $S = -1$  sector, there are four coupled channels with isospin  $I = 0$ , namely  $\pi\Sigma$ ,  $\bar{K}N$ ,  $\eta\Lambda$  and  $K\Xi$ . The various coefficients  $C_{M_j B_j, M_i B_i}^V$ ,  $C_{M_j B_j, M_i B_i}^B$  and  $\tilde{C}_{M_j B_j, M_i B_i}^B$  are tabulated in Tables I, II and III, where the indices  $i, j$  represent the particle channels. Here, we use the phase convention  $|\pi^+\rangle = -|1, 1\rangle$ ,  $|K^-\rangle = -|1/2, -1/2\rangle$ ,  $|\Sigma^+\rangle = -|1, 1\rangle$  and  $|\Xi^-\rangle = -|1/2, -1/2\rangle$  for the isospin states.

We rewrite the LO potential as the central and spin-orbital parts,

$$\begin{aligned}
 V_{M_j B_j, M_i B_i} &= V_{M_j B_j, M_i B_i}^{(a+b)} + V_{M_j B_j, M_i B_i}^{(c)} + V_{M_j B_j, M_i B_i}^{(d)} \\
 &\equiv W_{M_j B_j, M_i B_i}^c + i \boldsymbol{\sigma} \cdot (\mathbf{q}_2 \times \mathbf{q}_1) W_{M_j B_j, M_i B_i}^{so}.
 \end{aligned} \tag{9}$$

It is convenient to calculate the amplitude in the center-of-mass (CMS) frame with

$$\begin{aligned}
 q_1^\mu &= (\omega_{M_i}(\mathbf{p}), \mathbf{p}), & p_1^\mu &= (\omega_{B_i}(\mathbf{p}), -\mathbf{p}), \\
 q_2^\mu &= (\omega_{M_j}(\mathbf{p}'), \mathbf{p}'), & p_2^\mu &= (\omega_{B_j}(\mathbf{p}'), -\mathbf{p}'),
 \end{aligned} \tag{10}$$

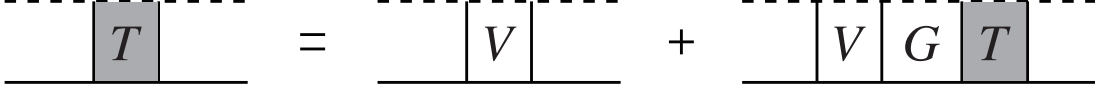


Figure 2: Diagrammatic representation of the meson-baryon scattering equation. The dashed and solid lines denote the pseudoscalar mesons and the octet baryons, respectively.

where the relative momenta  $\mathbf{p}$  and  $\mathbf{p}'$  are introduced. A state of the meson-baryon system can be represented as a sum of partial wave states, which are denoted as  $|LJ\rangle$ , where  $J$  is the total angular momentum and  $L = J \pm 1/2$  is the orbital angular momentum. Because of parity conservation in the strong interactions, the  $L_+ = J - 1/2$  and the  $L_- = J + 1/2$  waves are obviously decoupled. The partial wave projection of the potential in the isospin basis is given by

$$\begin{aligned} \langle L_{\pm}J|V_{M_j B_j, M_i B_i}|L_{\pm}J\rangle &\equiv V_{M_j B_j, M_i B_i}^{LJ} = \\ 2\pi \int_{-1}^1 dz &\left[ W_{M_j B_j, M_i B_i}^c P_{L_{\pm}}(z) + p^2 W_{M_j B_j, M_i B_i}^{so} P_{L_{\pm} \pm 1}(z) - zp^2 W_{M_j B_j, M_i B_i}^{so} P_{L_{\pm}}(z) \right], \end{aligned} \quad (11)$$

where  $z = \cos \theta$ , with  $\theta$  the angle between  $\mathbf{p}$  and  $\mathbf{p}'$ ,  $p \equiv |\mathbf{p}|$  and  $P_L(z)$  denotes the Legendre polynomial.

### C. Partial wave integral equations and subtractive renormalization

In time-ordered perturbation theory one obtains the coupled-channel integral equation for the  $T$ -matrix, which is visualized in Fig. 2,

$$\begin{aligned} T_{M_j B_j, M_i B_i}(\mathbf{p}', \mathbf{p}; E) &= V_{M_j B_j, M_i B_i}(\mathbf{p}', \mathbf{p}; E) \\ &+ \sum_{MB} \int \frac{d^3 \mathbf{k}}{(2\pi)^3} V_{M_j B_j, MB}(\mathbf{p}', \mathbf{k}; E) G_{MB}(E) T_{MB, M_i B_i}(\mathbf{k}, \mathbf{p}; E), \end{aligned} \quad (12)$$

where  $M_i B_i$ ,  $M_j B_j$  and  $MB$  denote the initial, final and intermediate particle channels, and the two-body Green functions read

$$G_{MB}(E) = \frac{1}{2\omega_M \omega_B} \frac{m_B}{E - \omega_M - \omega_B + i\epsilon}. \quad (13)$$

Projecting onto specific partial waves in the  $|LJ\rangle$  basis, the integral equation is written as

$$\begin{aligned} T_{M_j B_j, M_i B_i}^{LJ}(\mathbf{p}', \mathbf{p}; E) &= V_{M_j B_j, M_i B_i}^{LJ}(\mathbf{p}', \mathbf{p}; E) \\ &+ \sum_{MB} \int \frac{dk k^2}{(2\pi)^3} V_{M_j B_j, MB}^{LJ}(\mathbf{p}', \mathbf{k}; E) G_{MB}(E) T_{MB, M_i B_i}^{LJ}(\mathbf{k}, \mathbf{p}; E), \end{aligned} \quad (14)$$



where  $p$ ,  $p'$ ,  $k$  are defined as the magnitudes of the momenta,  $p = |\mathbf{p}|$ ,  $p' = |\mathbf{p}'|$ ,  $k = |\mathbf{k}|$ . Since the LO potential can be divided into the one-baryon-reducible and irreducible parts,

$$V_{M_j B_j, M_i B_i} = V_{M_j B_j, M_i B_i}^R + V_{M_j B_j, M_i B_i}^I, \quad (15)$$

with  $V^R = V^{(c)}$  and  $V^I = V^{(a+b)} + V^{(d)}$ , we can apply a subtractive renormalization to obtain the finite on-shell  $T$ -matrix. Using a symbolic notation, the meson-baryon integral equation  $T = V + VGT$  can be rewritten as a system of coupled equations as

$$\begin{aligned} T &= T_I + (1 + T_I G) T_R (1 + G T_I), \\ T_I &= V_I + V_I G T_I, \\ T_R &= V_R + V_R G (1 + T_I G) T_R. \end{aligned} \quad (16)$$

In order to obtain the renormalized finite T-matrix, we replace the meson-baryon propagator  $G_{MB}(E)$  with the subtracted one  $G_{MB}^S(E) = G_{MB}(E) - G_{MB}(m_B)$ . This corresponds to including the contributions of an infinite number of meson-baryon counter-terms (details can be found in Refs. [58, 59]). As discussed in Ref. [58], the subtractive renormalization does not affect the dynamics of bound states or resonances.

### III. RESULTS AND DISCUSSION

In the numerical evaluation, the masses of pseudoscalar mesons are taken as  $M_\pi = 138.0$  MeV,  $M_K = 495.6$  MeV, and  $M_\eta = 547.9$  MeV. For the masses of octet baryons we use  $m_N = 938.9$  MeV,  $m_\Lambda = 1115.6$  MeV,  $m_\Sigma = 1193.1$  MeV and  $m_\Xi = 1318.0$  MeV, while for the vector mesons the values  $M_\rho = 775.3$  MeV,  $M_{K^*} = 893.7$  MeV,  $M_\omega = 782.7$  MeV, and  $M_\phi = 1019.5$  MeV [5] are employed. The axial vector couplings are taken as  $D = 0.760$  and  $F = 0.507$ , with  $D + F = g_A = 1.267$ . The pseudoscalar decay constants are fixed as  $F_\pi = 92.07$  MeV,  $F_K = 110.1$  MeV and  $F_\eta \approx 1.2F_\pi$  according to the PDG average values [5]. Note that at this order, there is no free parameter (see also the discussion below). Thus, at this order we have pure predictions.

To obtain the  $I = 0$   $\bar{K}N$  scattering  $T$ -matrix with coupled-channel effects taken into account we need to solve the integral equation, Eq. (14), with the four coupled channels  $\bar{K}N$ ,  $\pi\Sigma$ ,  $\eta\Lambda$ , and  $K\Xi$ . Instead of introducing the approximation of the on-shell factorization (see, e.g., Ref. [43]), we solve the scattering equation with the full off-shell dependence. As argued in Refs. [37, 64, 65],

Table IV: Pole positions  $z_R$  of  $\Lambda(1405)$  in the  $S = -1$  sector (units are MeV).

		lower pole	higher pole
This work	$F_0 = F_\pi$	$1337.7 - i 79.1$	$1430.9 - i 8.0$
	(LO)	$F_0 = 103.4$	$1436.3 - i 0.7$
NLO	Ref. [35, 36]	$1381_{-6}^{+18} - i81_{-8}^{+19}$	$1424_{-23}^{+7} - i26_{-14}^{+3}$
	Ref. [38], Fit II	$1388_{-9}^{+9} - i114_{-25}^{+24}$	$1421_{-2}^{+3} - i19_{-5}^{+8}$
	Ref. [66], sol-2	$1330_{-5}^{+4} - i56_{-11}^{+17}$	$1434_{-2}^{+2} - i10_{-1}^{+2}$
	Ref. [66], sol-4	$1325_{-15}^{+15} - i90_{-18}^{+12}$	$1429_{-7}^{+8} - i12_{-3}^{+2}$

this treatment is necessary since the pole positions of resonances can change in solving the Bethe-Salpeter equation with the full off-shell dependence of the chiral potential. Then, using the S-wave projection of the chiral LO potential of Eq. (8), we employ the subtractive renormalization to obtain the finite S-wave  $T$ -matrix that does not contain contributions increasing with the cutoff  $\Lambda$ , i.e. one can take the limit  $\Lambda \rightarrow \infty$ .<sup>1</sup> It is worth noticing that our framework does not have the usual obstacle of the large cutoff-dependence of the  $T$ -matrix present in the traditional chiral unitary approach.

Performing an analytic continuation of the  $T$ -matrix into the complex  $s$ -plane, we find the  $\Lambda(1405)$  resonance with the two-pole structure in the second Riemann sheet with only the  $\pi\Sigma$  channel open for decay (i.e.  $(M_\pi + m_\Sigma)^2 < s < (M_{\bar{K}} + m_N)^2$ ). The obtained pole positions are denoted as the “lower” pole and “higher” pole and listed in Table IV. By varying the meson-decay constant,  $F_0$ , from the physical SU(2) value  $F_\pi = 92.07$  MeV to its SU(3)-average value 103.4 MeV, we find that the width of the first pole is increasing. The second pole lies close and moves beyond the threshold of  $\bar{K}N$  channel, and its width decreases, when the meson decay constant increases. Our LO results are consistent with the ones of the NLO study of Ref. [66], in particular, for what concerns the results for the lower pole.

It is further interesting to investigate the structure of the above two poles. Approaching the pole position  $z_R$ , the on-shell scattering  $T$ -matrix can be approximated by

$$T_{ij} \simeq 4\pi \frac{g_i g_j}{z - z_R}, \quad (17)$$

where  $g_i$  ( $g_j$ ) represents the contribution to the coupling strength of the initial (final) transition

<sup>1</sup> In practice, we prefer to choose finite cutoff values like  $\Lambda = 10$  GeV that are sufficiently large to keep finite- $\Lambda$  artifacts negligibly small.

Table V: The (absolute) values of the coupling strengths  $g_i$  ( $|g_i|$ ) for the two poles of  $\Lambda(1405)$  resonance.

	lower pole		higher pole	
	$g_i$	$ g_i $	$g_i$	$ g_i $
$\pi\Sigma$	$1.83 + i1.90$	2.64	$-0.38 + i0.84$	0.92
$\bar{K}N$	$-1.59 - i1.47$	2.17	$2.16 - i0.83$	2.31
$\eta\Lambda$	$-0.19 - i0.67$	0.69	$1.59 - i0.36$	1.63
$K\Xi$	$0.72 + i0.81$	1.08	$-0.10 + i0.34$	0.35

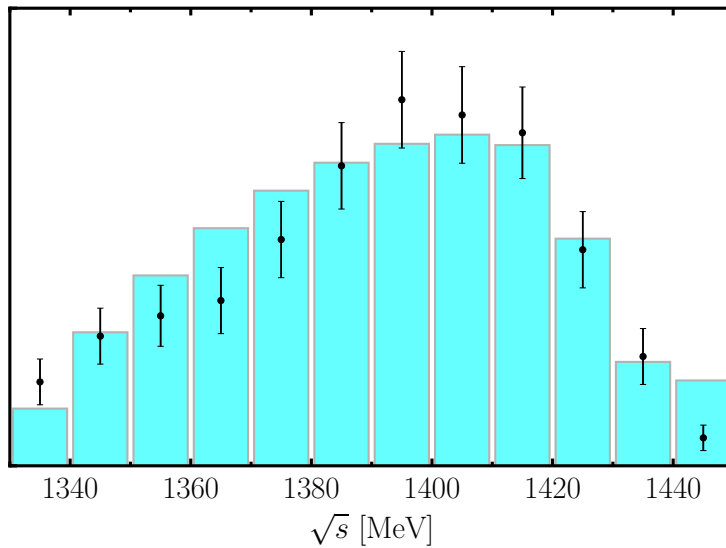


Figure 3:  $\pi\Sigma$  invariant mass spectrum with  $I = 0$  in arbitrary units. The histogram represents the result of our calculations as explained in the text. Experimental data for the  $\pi^-\Sigma^+$  event distribution are taken from Ref. [67].

channel. In general, the couplings  $g_i$ ,  $g_j$ , which can be extracted from the residues of the  $T$ -matrix, are complex-valued numbers. The couplings obtained for the  $\Lambda(1405)$  resonance are tabulated in Table V. One can see that the lower pole couples predominantly to the  $\pi\Sigma$  channel, while the higher pole couples strongly to the  $\bar{K}N$  channel. This could explain the large imaginary part of the lower pole, which is the consequence of the strong  $\pi\Sigma$  coupling. Thus, the different coupling nature to the meson-baryon channels form the two-pole structure of  $\Lambda(1405)$ .

Furthermore, we present the shape of the  $\Lambda(1405)$  spectrum in Fig. 3, where the calculated invariant mass distribution is compared with the experimental data of  $\pi^-\Sigma^+$  channel from Ref. [67].

The event distribution is calculated by taking into account both the  $\pi\Sigma \rightarrow \pi\Sigma$  and  $\bar{K}N \rightarrow \pi\Sigma$  channels as described in Ref. [27].

Finally, we note that we have also calculated the  $\bar{K}N$  scattering lengths for  $I = 0$  and  $I = 1$ . The isospin-zero scattering length turns out to be  $a_0 = -2.50 + i1.37$  fm, which is somewhat outside of the region allowed by combining the scattering data with the SIDDHARTA kaonic hydrogen result, see e.g. Ref. [68]. We expect this issue to be resolved upon including NLO corrections. Our LO result for the isovector scattering length  $a_1 = 0.33 + i0.72$  fm is, on the other hand, within the allowed region mapped out from scattering and kaonic hydrogen data.

#### IV. SUMMARY AND OUTLOOK

In this paper we have studied meson-baryon scattering in the strangeness  $S = -1$  sector to investigate the structure of the  $\Lambda(1405)$  resonance using time-ordered perturbation theory applied to the Lorentz-invariant effective chiral Lagrangian with the explicit inclusion of low-lying vector mesons. In the considered framework, the effective potential of the meson-baryon scattering is defined as a sum of two-particle irreducible time-ordered diagrams. The renormalized S-wave amplitudes with  $I = 0$  are obtained by taking into account the full off-shell dependence of the potential in the coupled-channel integral equations and applying subtractive renormalization.

In our leading-order study with no free parameters, we obtain the two-pole structure of the  $\Lambda(1405)$  state. The higher pole at  $E_R = 1431 - i8$  MeV is mainly coupled to the  $\bar{K}N$  channel, while the lower one located at  $E_R = 1338 - i79$  MeV couples mainly to the  $\pi\Sigma$  channel. It is worth noticing that our results are independent on the momentum cutoff. The obtained  $\pi\Sigma$  invariant mass distribution agrees well with the experimental data while the  $\bar{K}N$  isoscalar scattering length is found to have a somewhat too large (in magnitude) real part.

The existing data and the upcoming experiments focused on investigating the  $\bar{K}N$  dynamics, such as the lowest-energy beam of strange hadron production in JLab experiments [69], the kaonic hydrogen SIDDHARTA experiment [15], the photoproduction data from JLab [70] and the experiments with kaonic nuclear bound states [71, 72] provide a strong motivation to extend our renormalizable framework to next-to-leading order. Work along these lines is in progress.

## Acknowledgements

This work was supported in part by BMBF (Grant No. 05P18PCFP1), by DFG and NSFC through funds provided to the Sino-German CRC 110 “Symmetries and the Emergence of Structure in QCD” (NSFC Grant No. 11621131001, Project-ID 196253076 - TRR 110), by Collaborative Research Center “The Low-Energy Frontier of the Standard Model” (DFG, Project No. 204404729 - SFB 1044), by the Cluster of Excellence “Precision Physics, Fundamental Interactions, and Structure of Matter” (PRISMA<sup>+</sup>, EXC 2118/1) within the German Excellence Strategy (Project ID 39083149), by the Georgian Shota Rustaveli National Science Foundation (Grant No. FR17-354), by VolkswagenStiftung (Grant No. 93562), by the CAS President’s International Fellowship Initiative (PIFI) (Grant No. 2018DM0034) and by the EU (STRONG2020).

- 
- [1] B. P. Abbott *et al.* [LIGO Scientific and Virgo], *Phys. Rev. Lett.* **119**, 161101 (2017); *Phys. Rev. X* **9**, 011001 (2019).
  - [2] D. B. Kaplan and A. E. Nelson, *Phys. Lett. B* **175**, 57-63 (1986)
  - [3] S. Pal, D. Bandyopadhyay and W. Greiner, *Nucl. Phys. A* **674**, 553-577 (2000).
  - [4] D. Gazda, E. Friedman, A. Gal and J. Mares, *Phys. Rev. C* **76**, 055204 (2007) [erratum: *Phys. Rev. C* **77**, 019904 (2008)].
  - [5] P. A. Zyla *et al.* [Particle Data Group], *PTEP* **2020**, 083C01 (2020).
  - [6] R. H. Dalitz and S. F. Tuan, *Phys. Rev. Lett.* **2**, 425-428 (1959); *Annals Phys.* **10**, 307-351 (1960).
  - [7] M. H. Alston, L. W. Alvarez, P. Eberhard, M. L. Good, W. Graziano, H. K. Ticho and S. G. Wojcicki, *Phys. Rev. Lett.* **6**, 698-702 (1961).
  - [8] P. L. Bastien, M. Ferro-Luzzi and A. H. Rosenfeld, *Phys. Rev. Lett.* **6**, 702 (1961).
  - [9] W. E. Humphrey and R. R. Ross, *Phys. Rev.* **127**, 1305-1323 (1962).
  - [10] M. B. Watson, M. Ferro-Luzzi and R. D. Tripp, *Phys. Rev.* **131**, 2248-2281 (1963).
  - [11] M. Sakitt, T. B. Day, R. G. Glasser, N. Seeman, J. H. Friedman, W. E. Humphrey and R. R. Ross, *Phys. Rev.* **139**, B719 (1965).
  - [12] J. Ciborowski, J. Gwizdz, D. Kielczewska, R. J. Nowak, E. Rondio, J. A. Zakrzewski, M. Goossens, G. Wilquet, N. H. Bedford and D. Evans, *et al.* *J. Phys. G* **8**, 13-32 (1982).
  - [13] D. N. Tovee, D. H. Davis, J. Simonovic, G. Bohm, J. Klabuhn, F. Wysotzki, M. Csejthey-Barth,

- J. H. Wickens, T. Cantwell and C. Ni Ghogain, *et al.* Nucl. Phys. B **33**, 493-504 (1971).
- [14] R. J. Nowak, J. Armstrong, D. H. Davis, D. J. Miller, D. N. Tovee, D. Bertrand, M. Goossens, G. Vanhomwegen, G. Wilquet and M. Abdullah, *et al.* Nucl. Phys. B **139**, 61-71 (1978).
- [15] M. Bazzi *et al.* [SIDDHARTA collaboration], Phys. Lett. B **704**, 113-117 (2011).
- [16] J. W. Darewych, R. Koniuk and N. Isgur, Phys. Rev. D **32**, 1765 (1985).
- [17] L. S. Kisslinger and E. M. Henley, Eur. Phys. J. A **47**, 8 (2011).
- [18] P. B. Siegel and W. Weise, Phys. Rev. C **38**, 2221-2229 (1988).
- [19] P. J. Fink, Jr., G. He, R. H. Landau and J. W. Schnick, Phys. Rev. C **41**, 2720-2725 (1990).
- [20] A. Cieply and J. Smejkal, Nucl. Phys. A **881**, 115-126 (2012).
- [21] A. Cieplý and V. Krejčířík, Nucl. Phys. A **940**, 311-330 (2015).
- [22] K. Miyahara, T. Hyodo and W. Weise, Phys. Rev. C **98**, 025201 (2018).
- [23] T. Ezo and A. Hosaka, Phys. Rev. D **102**, 014046 (2020).
- [24] Z.-W. Liu, J. M. M. Hall, D. B. Leinweber, A. W. Thomas and J. J. Wu, Phys. Rev. D **95**, 014506 (2017).
- [25] N. Kaiser, P. B. Siegel and W. Weise, Nucl. Phys. A **594**, 325-345 (1995).
- [26] E. Oset and A. Ramos, Nucl. Phys. A **635**, 99-120 (1998).
- [27] J. A. Oller and U.-G. Meißner, Phys. Lett. B **500**, 263-272 (2001).
- [28] M. F. M. Lutz and E. E. Kolomeitsev, Nucl. Phys. A **700**, 193-308 (2002).
- [29] T. Hyodo, S. I. Nam, D. Jido and A. Hosaka, Phys. Rev. C **68**, 018201 (2003).
- [30] C. Garcia-Recio, J. Nieves, E. Ruiz Arriola and M. J. Vicente Vacas, Phys. Rev. D **67**, 076009 (2003).
- [31] D. Jido, J. A. Oller, E. Oset, A. Ramos and U.-G. Meißner, Nucl. Phys. A **725**, 181-200 (2003).
- [32] B. Borasoy, R. Nissler and W. Weise, Eur. Phys. J. A **25**, 79-96 (2005).
- [33] B. Borasoy, U.-G. Meißner and R. Nissler, Phys. Rev. C **74**, 055201 (2006).
- [34] J. A. Oller, Eur. Phys. J. A **28**, 63-82 (2006).
- [35] Y. Ikeda, T. Hyodo and W. Weise, Phys. Lett. B **706**, 63-67 (2011).
- [36] Y. Ikeda, T. Hyodo and W. Weise, Nucl. Phys. A **881**, 98-114 (2012).
- [37] M. Mai and U.-G. Meißner, Nucl. Phys. A **900**, 51 - 64 (2013).
- [38] Z. H. Guo and J. A. Oller, Phys. Rev. C **87**, 035202 (2013).
- [39] A. Cieplý, M. Mai, U.-G. Meißner and J. Smejkal, Nucl. Phys. A **954**, 17-40 (2016).
- [40] Y. Kamiya, K. Miyahara, S. Ohnishi, Y. Ikeda, T. Hyodo, E. Oset and W. Weise, Nucl. Phys. A **954**, 41-57 (2016).

- [41] D. Sadasivan, M. Mai and M. Döring, Phys. Lett. B **789**, 329-335 (2019).
- [42] A. Feijoo, V. Magas and A. Ramos, Phys. Rev. C **99**, 035211 (2019).
- [43] T. Hyodo and D. Jido, Prog. Part. Nucl. Phys. **67**, 55-98 (2012).
- [44] A. Gal, E. V. Hungerford and D. J. Millener, Rev. Mod. Phys. **88**, 035004 (2016).
- [45] L. Tolos and L. Fabbietti, Prog. Part. Nucl. Phys. **112**, 103770 (2020).
- [46] M. Mai, [[arXiv:2010.00056](https://arxiv.org/abs/2010.00056) [nucl-th]].
- [47] B. J. Menadue, W. Kamleh, D. B. Leinweber and M. S. Mahbub, Phys. Rev. Lett. **108**, 112001 (2012).
- [48] G. P. Engel *et al.* [BGR], Phys. Rev. D **87**, 074504 (2013).
- [49] J. M. M. Hall, W. Kamleh, D. B. Leinweber, B. J. Menadue, B. J. Owen, A. W. Thomas and R. D. Young, Phys. Rev. Lett. **114**, 132002 (2015).
- [50] S. Weinberg, Physica A **96**, , 327-340 (1979).
- [51] J. Gasser and H. Leutwyler, Nucl. Phys. B **250**, 465-516 (1985).
- [52] U.-G. Meißner, Symmetry **12**, 981 (2020).
- [53] F. Y. Dong, B. X. Sun and J. L. Pang, Chin. Phys. C **41**, no. 7, 074108 (2017).
- [54] J. Révai, Few Body Syst. **59**, 49 (2018).
- [55] K. S. Myint, Y. Akaishi, M. Hassanvand and T. Yamazaki, PTEP **2018**, no.7, 073D01 (2018).
- [56] P. C. Bruns and A. Cieplý, Nucl. Phys. A **996**, 121702 (2020).
- [57] A. V. Anisovich, A. V. Sarantsev, V. A. Nikonov, V. Burkert, R. A. Schumacher, U. Thoma and E. Klempt, Eur. Phys. J. A **56**, 139 (2020).
- [58] X.-L. Ren, E. Epelbaum, J. Gegelia and U.-G. Meißner, Eur. Phys. J. C **80**, 406 (2020).
- [59] E. Epelbaum, A. M. Gasparyan, J. Gegelia, U.-G. Meißner and X.-L. Ren, Eur. Phys. J. A **56**, 152 (2020).
- [60] X.-L. Ren, E. Epelbaum and J. Gegelia, Phys. Rev. C **101**, 034001 (2020).
- [61] V. Baru, E. Epelbaum, J. Gegelia and X.-L. Ren, Phys. Lett. B **798**, 134987 (2019).
- [62] P. C. Bruns and U.-G. Meißner, Eur. Phys. J. C **40**, 97-119 (2005).
- [63] B. Kubis and U.-G. Meißner, Nucl. Phys. A **679**, 698-734 (2001).
- [64] P. C. Bruns, M. Mai and U.-G. Meißner, Phys. Lett. B **697**, 254-259 (2011).
- [65] O. Morimatsu and K. Yamada, Phys. Rev. C **100**, no.2, 025201 (2019).
- [66] M. Mai and U.-G. Meißner, Eur. Phys. J. A **51**, 30 (2015).
- [67] R. J. Hemingway, Nucl. Phys. B **253**, 742-752 (1985).
- [68] M. Döring and U.-G. Meißner, Phys. Lett. B **704**, 663 (2011).

- [69] M. Amaryan *et al.* [KLF collaboration], [[arXiv:2008.08215](https://arxiv.org/abs/2008.08215) [nucl-ex]].
- [70] K. Moriya *et al.* [CLAS collaboration], Phys. Rev. C **87**, no.3, 035206 (2013).
- [71] M. Miliucci, A. Amirkhani, A. Baniahmad, M. Bazzi, D. Bosnar, M. Bragadireanu, M. Carminati, M. Cargnelli, C. Curceanu and A. Clozza, *et al.* Acta Phys. Polon. Supp. **14**, 49 (2021).
- [72] F. Sakuma *et al.* [JPARC-E 015], JPS Conf. Proc. **32**, 010088 (2020).